

# Scaling Methods To Estimate Macroscopic Fundamental Diagrams in Urban Networks with Sparse Sensor Coverage

Nandan Maiti<sup>a</sup>, Manon Seppecher<sup>a</sup>, Ludovic Leclercq<sup>a</sup>

<sup>a</sup>*Univ. Eiffel, ENTPE, LICIT-ECO7, Lyon, 69500, France*

---

## Abstract

Accurately estimating traffic variables across unequipped portions of a network remains a significant challenge due to the limited amount of sensors-equipped links, such as loop detectors and probe vehicles. A common approach is to apply uniform scaling, treating unequipped links as equivalent to equipped ones, which leads to a strong bias in MFD estimation. Two main approaches are proposed: (1) Hierarchical Network Scaling and (2) Variogram-based data imputation. The hierarchical scaling method categorizes the network into several clusters according to spatial and functional characteristics, applying tailored scaling factors to each category. The variogram-based imputation leverages spatial correlations to estimate traffic variables for unequipped links, capturing spatial dependencies in urban road networks. Validation results show that the hierarchical scaling approach yields the most accurate estimates, demonstrating reliable performance with as little as 5% uniform detector coverage, while the variogram model fails to provide estimates. While the variogram-based method provides strong results with over 10% detector coverage, it is slightly less effective than the hierarchical scaling approach but performs better than the baseline non-hierarchical method.

*Keywords:* Network scaling, Macroscopic fundamental diagrams, Spatial imputation, Loop detectors, Equipped networks.

---

## 1. Introduction

The Macroscopic Fundamental Diagrams (MFDs) has emerged as a critical tool in network traffic management, providing a relationship between aggregate traffic variables such as flow, density, and speed across an entire urban road network (Daganzo and Geroliminis, 2008). This concept offers valuable insights for network traffic control (Keyvan-Ekbatani et al., 2015; Ampountolas et al., 2017), particularly in perimeter control strategies (Aboudolas and Geroliminis, 2013; Mariotte and Leclercq, 2019; Jiang and Keyvan-Ekbatani, 2023), where traffic inflow and outflow are managed to optimize network-wide performances. By monitoring traffic at a macroscopic level, the MFDs enable decision-makers

to regulate traffic in real time, improve congestion management, and enhance the overall efficiency of urban transportation systems.

Despite its potential, estimating reliable MFDs for a city network requires extensive empirical data. Loop detector device (LDD), the most commonly used data source for MFDs estimation, collects information from fixed sensors embedded in road infrastructure (Buisson and Ladier, 2009; Geroliminis and Sun, 2011; Keyvan-Ekbatani et al., 2012; Saberi and Mahmassani, 2012; Aboudolas and Geroliminis, 2013; Keyvan-Ekbatani et al., 2013; Ambühl et al., 2021; Lee et al., 2023; Mousavizadeh and Keyvan-Ekbatani, 2024). However, LDD faces limitations, such as positional biases in speed estimation (Leclercq et al., 2014; Maiti, 2024), and uneven distribution of sensors in a network (Lee et al., 2023), leading to incomplete coverage. To address these limitations, floating-car devices (FCD), or probe is often used alongside LDD to enhance spatial coverage, primarily for improving spatial speed estimation (Geroliminis and Daganzo, 2008; Gayah and Daganzo, 2011; Geroliminis and Sun, 2011; Mahmassani et al., 2013; Tsubota et al., 2014; Ambühl and Menendez, 2016; Yang Beibei et al., 2016; Du et al., 2016; Saeedmanesh and Geroliminis, 2016; Ambühl et al., 2017; Dakic and Menendez, 2018; Mariotte et al., 2020a,b). However, FCD has its own challenges, including the unknown and variable penetration rate of vehicles equipped with GPS in time and space. Estimating network-wide traffic flows based on the assumption of homogeneous FCD penetration introduces uncertainty in the flow estimation, particularly when coverage is sparse (Leclercq et al., 2014; Shim et al., 2019; Fu et al., 2020).

The limitations of these data sources underscore a broader issue: the network-wide traffic data used for MFD estimation is typically incomplete. LDD and FCD are often available only for certain links in the network, resulting in what is known as an ‘equipped network MFD’, an MFD that only reflects the links where sensors or FCD are deployed (Mariotte et al., 2020a). Consequently, this equipped MFD may not be representative of the entire network. This is critical for simulation studies as the demand is usually given for the full region, and estimating capacity and other variables on the equipped network only creates a mismatch with trips that could totally or partially happen in the non-equipped network.

To scale the equipped network MFD to the full city network, previous studies have attempted to partition the network into homogeneous areas and apply a scaling factor that adjusts for the ratio between the total length of links in the network and the length of the equipped links, e.g., Mariotte et al. (2020a). While this approach can offer some level of approximation, it suffers from significant limitations. The partitioning of the network based on equipped network data can lead to erroneous estimations of homogeneous areas, as the unequipped links may exhibit different traffic characteristics (Jiang et al., 2023; Jiang and Keyvan-Ekbatani, 2023; Saeedmanesh and Geroliminis, 2016, 2017; Gu and Saberi, 2019; Johari et al., 2023). Furthermore, applying a uniform scaling factor across areas with varying types of links, such as arterials and local roads, may lead to inaccurate flow estimates.

There is a need for a more advanced approach to spatial scaling of the MFD.

To overcome the challenges associated with uniform scaling, a new methodology that accounts for the link hierarchy within a network is proposed. This method involves developing separate scaling factors for different hierarchical levels of the network, such as major arterials, collectors, and local streets. By accounting for the differences in traffic behavior at various link levels, this approach offers a more accurate estimation of network flow variables, allowing for accurate scaling of MFD from sensor-equipped portions of the network to the entire city.

### 1.1. Literature Review

#### 1.1.1. Equipped Networks' MFDs

The literature about MFD estimation from 'equipped network' to 'full network' can be broadly classified into two groups based on the data used: one using empirical data sources from the equipped network, the other relying on large-scale simulation frameworks for a city. The main challenges associated with the empirical data are the limited coverage of LDD and FCD throughout the network, while the simulations fail to replicate the multimodal interactions and traffic dynamics of a complex network (Leclercq et al., 2014; Mariotte et al., 2020b; Maiti and Chilukuri, 2023). Thus, we mainly focused on the existing empirical study on MFD estimation and calibration.

MFD estimation predominantly relied on LDD (Geroliminis and Daganzo, 2008; Buisson and Ladier, 2009) information on vehicle counts and occupancy rates on road segments, allowing the calculation of network-wide average flow and density. This approach was inspired by Edie (1963) definition of traffic flow metrics, where average flow and density are calculated based on the data collected from multiple equipped links within a network (Leclercq et al., 2014). However, the reliance on LDD has certain limitations. LDD is an Eulerian observation method, which may introduce bias in MFD estimation, particularly due to the spatial distribution of detectors (Leclercq et al., 2014). The placement of detectors, often in congested areas or near traffic signals, can result in an overestimation of network density (Lee et al., 2023; Maiti, 2024). Despite this limitation, studies have shown that MFDs derived from a small fraction of links can still approximate critical density ranges observed in the full network MFD (Keyvan-Ekbatani et al., 2013). Mariotte et al. (2020a) introduced the concept of an 'active network' to improve MFD estimation, focusing on major arterials and secondary roads. They highlighted the importance of scaling the production MFD based on the ratio of total network length to equipped network length. The estimated scaling factor for production is based on the assumption of homogeneous network partitioning (Zheng and Geroliminis, 2013; Saeedmanesh and Geroliminis, 2016, 2017; Jiang et al., 2023; Johari et al., 2023) using the equipped network information, leading to ambiguity in partitioning for full network. Saffari et al. (2020) expanded on this by investigating the selection of critical links for MFD estimation, though they noted that their findings were sensitive to the specific test bed used.

There are two main options for estimating the traffic states in non-equipped networks to derive complete MFDs. The first involves grouping non-equipped

links with clusters of links exhibiting similar behavior and determining a scaling factor for each cluster. The second approach focuses on imputing missing link variables for non-equipped links. The following review outlines the existing studies for spatial scaling and imputation in network traffic state estimation.

### 1.1.2. Spatial Scaling

The main challenge with imputing traffic states at the unequipped links is the estimation errors due to a lack of available information from the surrounding links and heterogeneity of traffic states among links. Network traffic state estimation approaches can be broadly classified into two main categories: model-driven and data-driven (Seo et al., 2017; Takayasu et al., 2022). High-accuracy model-driven methods often require additional information, such as detailed traffic signal settings or individual vehicle detector actuation data (Wu et al., 2011; Leclercq et al., 2014). While these methods have proven efficient in estimating traffic states, particularly at the link level (Nantes et al., 2016; Maiti and Chilukuri, 2024; Maiti et al., 2024; Maiti and Chilukuri, 2023), their accuracy is highly dependent on the quality of the embedded models. Data-driven approaches leverage large amounts of historical data to train models using machine learning or statistical techniques (Qing-Jie Kong et al., 2009; Anuar et al., 2015; Lu et al., 2018; Takayasu et al., 2022; Maiti and Chilukuri, 2023). Since data-driven methods do not rely on strict theoretical assumptions, the accuracy of the models is largely influenced by the quantity and quality of the data. However, missing data is a common issue in data-driven methods, and several studies have attempted to address this problem (Chen et al., 2003; Xu et al., 2015; Offor et al., 2019). Nowadays, graph convolution networks (GCN), generative adversarial networks (GANs), and physics-informed neural networks (PINNs) are gaining significant attention in estimating the missing traffic flow variables in unequipped networks. GCNs struggle with capturing dynamic temporal changes in traffic networks, as they are often designed for static graphs. Additionally, the hierarchical and complex topology of traffic networks complicates model training (Rossi et al., 2021; Taguchi et al., 2021; Castro-Correa et al., 2023; Bao et al., 2023; Zhang et al., 2023). GANs face difficulties generating realistic traffic data due to the stochastic nature of traffic demand, making adversarial training unstable (Zhang et al., 2019; Zheng et al., 2022). PINNs, while incorporating physical laws, may struggle with noisy or incomplete data, as real-world traffic patterns can deviate significantly from theoretical models (Zhang et al., 2024; Usama et al., 2022). Balancing accuracy and computational efficiency remains a significant challenge across these approaches.

### 1.1.3. Geo-spatial imputation

In transportation data, kriging has been used to impute missing values in Annual Average Daily Traffic (AADT) datasets, with studies showing its superiority over traditional regression models like ordinary least squares (OLS) (Eom et al., 2006; Wang and Kockelman, 2009). The kriging method outperformed OLS, particularly in regions with moderate-to-high traffic volumes.



However, under low traffic flow conditions, it tends to overestimate the missing data (Wang and Kockelman, 2009). One of the limitations of the Kriging method is its reliance on Euclidean distance, which may not be ideal for transportation networks where distances are more appropriately measured along road networks. Zou et al. (2012) proposed the use of an approximated road network distance based on isometric embedding theory to address this issue, improving the interpolation accuracy, particularly in complex road networks. Nevertheless, studies such as Selby and Kockelman (2013) indicated that the use of road network distances does not always significantly improve prediction performance compared to traditional Euclidean distance-based methods.

In addition, while kriging has demonstrated success in spatial imputation, its application to spatio-temporal data remains relatively underexplored. Some studies, such as those by Yang et al. (2014), have extended kriging to account for both spatial and temporal dimensions. These efforts aim to better capture the spatio-temporal characteristics of traffic data. Moreover, Marcotte (1991) proposed cokriging, which uses secondary correlated variables alongside the primary variable, has shown promise in various fields. The application of cokriging for traffic data imputation is an area worth exploring, especially given the availability of multiple sources of traffic data (Shamo et al., 2015). A recent study by Bae et al. (2018) proposed the use of spatiotemporal cokriging to impute missing traffic flow speed data, integrating multiple data sources. Their results demonstrate that spatiotemporal cokriging improves the accuracy of imputation, particularly when missing data exhibit non-random patterns, such as blocks of missing data, which occur due to system malfunctions or maintenance issues. Later, Laval (2023) showed that the traffic flow variables such as travel times, relaxation times, and delay in urban networks near critical density follow the scaling with total network length.

Despite the advancements in using the MFD for traffic management, several gaps remain. Current methods rely on incomplete data from LDD and FCD, leading to inaccurate MFD estimates that do not fully represent the entire network. Uniform scaling approaches overlook the hierarchical nature of urban road networks, resulting in imprecise flow and density estimates across different road types. Additionally, advanced data-driven models like GCNs and PINNs struggle with missing or noisy data, limiting their effectiveness in estimating traffic states. Moreover, traditional spatial scaling techniques such as kriging are not well-explored for complex road networks. A more refined approach, incorporating link-hierarchical scaling and better data imputation, is needed to improve MFD accuracy for complete network estimation. This study develops a comprehensive framework for scaling network flow dynamics from equipped to full networks by incorporating road hierarchy and spatial imputation techniques. The main contributions of this study are listed below:

1. This work includes a novel hierarchical network scaling framework, which accounts for the distinct traffic characteristics of different road types, such as arterials and local streets, overcoming the inaccuracies of uniform scaling methods.

2. Utilizes geospatial imputation methods, such as variogram models, for network traffic data imputation. It leverages secondary data sources to fill gaps and inconsistencies in LDD coverage, ensuring a more accurate estimation of network traffic dynamics.
3. Provides validation of the proposed methodologies using real-world traffic data, demonstrating their effectiveness in capturing network-wide traffic dynamics.

## 2. Methodology

The proposed methodology estimates traffic variables for an entire network based on partially sensor-equipped data using hierarchical network scaling and variogram-based imputation approaches. Initially, the network is classified into equipped and unequipped links. In the hierarchical approach, links are categorized into several hierarchical levels based on spatial and functional characteristics, with tailored scaling factors applied to estimate traffic on unequipped links on each hierarchy. The spatial imputation approach employs variogram-based imputation to model spatial correlations between equipped and unequipped links, refining the traffic estimates. The outputs from these methods provide comprehensive estimates of traffic variables across the network, integrating observed data with imputed values for unequipped links. The results are benchmarked against a non-hierarchical uniform scaling method, which applies consistent scaling factors across all links regardless of their spatial or functional characteristics. A summary of the methodological framework is provided in Figure 1.

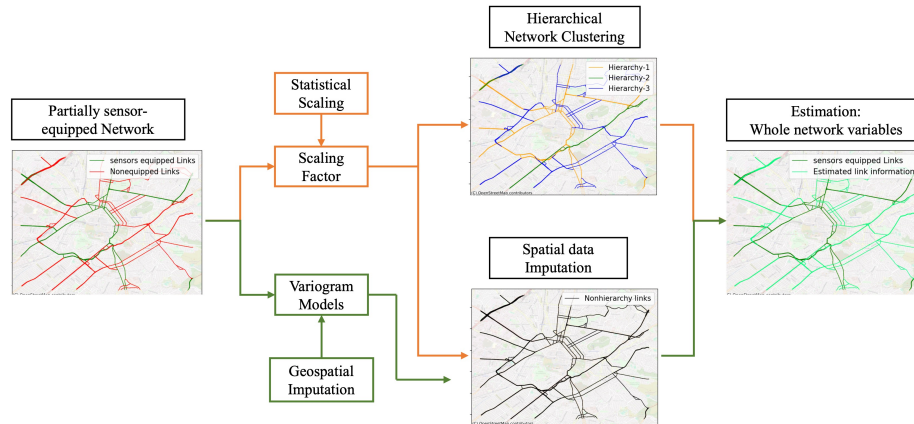


Figure 1: An overview of the overall methodology for estimating whole network variables from the partially-equipped network

## 2.1. Network Variables Estimation and Scaling Issues

### 2.1.1. Uniform Scaling or Baseline

Let's assume a traffic network having links ( $i$ ) of  $n$  numbers ( $|i| = n$ ), with a different hierarchy based on serviceability, defined as link class as  $t$ . Among all the links, some have loop detectors (LDs) count as  $j$ . Therefore, the flow in the links of LDs can be presented as  $\{q_j \mid j \in i\}$ . The lengths of the links in the network are represented by  $l_i$ . The overall network flow ( $\hat{q}_N$ ) can be expressed by total travel distance (TTD) as network 'production' by all vehicles over the time-space region, shown as follows in (1):

$$\hat{q}_N = \frac{\sum_{i=1}^n TTD_i}{\sum_{i=1}^n l_i \Delta t} \quad (1)$$

The TTD is the sum of equipped network TTD ( $TTD_{j,eq}$ ) and non-equipped network TTD ( $TTD_{i \notin i, neq}$ )

$$TTD = \sum_{i=1}^n TTD_i = \sum_{\forall j \in \{eq\}} TTD_{j,eq} + \sum_{\forall i \in \{neq\}} TTD_{i,neq} \quad (2)$$

The first term of (2) can be calculated from the LDs.

$$\sum_{\forall j \in \{eq\}} TTD_{j,eq} = \sum_{\forall j \in \{eq\}} q_j l_j \quad (3)$$

The second term of (2) can be directly estimated after the imputation method. Otherwise, we know that the following expectation relation holds for all situations.

$$\mathbb{E}(q_i l_i) = \mathbb{E}(q_i) \mathbb{E}(l_i) + Cov(q_i, l_i) \quad (4a)$$

$$\frac{1}{p} \sum_{i \in \{neq\}} (q_i l_i) = \left( \frac{1}{p} \sum_{i \in \{neq\}} q_i \right) \frac{1}{p} \sum_{i \in \{neq\}} l_i + Cov_{neq}(q_i, l_i) \quad (4b)$$

$$\sum_{i \in \{neq\}} (q_i l_i) = \bar{q}_{neq} \sum_{i \in \{neq\}} l_i + p \times Cov_{neq}(q_i, l_i) \quad (4c)$$

Here,  $\bar{q}_{neq}$  is the mean flow in the non-equipped network, and  $p$  is the total number of non-equipped links ( $|i \notin j| = p$ ). Also, assume  $m$  is the total number of equipped links ( $|j| = m$ ) in the network with mean flow estimated as  $\bar{q}_{eq}$  from LDs. If we assume the non-equipped network shares the same average flow and covariance as the equipped, then we can calculate the second term of (2), as (5).

$$\sum_{\forall i \in \{neq\}} (q_i l_i) = \bar{q}_{neq} \sum_{\forall i \in \{neq\}} l_i + p \times Cov_{neq}(q_i, l_i) \quad (5a)$$

$$= \left( \frac{1}{m} \sum_{j \in \{eq\}} q_j \right) \sum_{\forall i \in \{neq\}} l_i + p \times Cov_{eq}(q_j, l_j) \quad (5b)$$

$$= \bar{q}_{eq} \sum_{\forall i \in \{neq\}} l_i + p \times Cov_{eq}(q_j, l_j) \quad (5c)$$

Note the covariance term can be disregarded as it was proven negligible in all our data analysis. So, the TTD can be expressed as

$$TTD = \bar{q}_{eq} \times \left( \sum_{\forall i \in \{neq\}} l_i + \sum_{\forall j \in \{eq\}} l_j \right) \quad (6a)$$

$$= \bar{q}_{eq} \times l_{net} \quad (6b)$$

Here  $l_{net}$  is the total network length, including equipped and non-equipped links. The assumption,  $\bar{q}_{neq} = \bar{q}_{eq}$  forms the foundation of the uniform scaling factor, where all variables are scaled by the factor of network length covered.

Unfortunately, this assumption is often invalid, and equipped links are not a randomly selected subset of the full network. We propose a hierarchical scaling approach that will cluster the equipped network into groups that more likely resemble parts of the non-equipped network.

### 2.1.2. Hierarchical Network Scaling

The general idea in the hierarchical network scaling method is that we want to approach  $\bar{q}_{neq} = \bar{q}_{eq}$  at the cluster level. Similar to (5), we can use the  $\bar{q}_{eq,t}$  to estimate the  $\bar{q}_{neq,t}$ , where  $t$  represents link clusters. One option is to use the network hierarchy to define the clusters. Thus, we propose the following scaling method for the hierarchical network approach.

$$\sum_{\forall t} TTD_{eq,t} = \sum_{\forall j,t} q_{j,t} l_{j,t} \quad (7)$$

$$\mathbb{E}(q_{j,t} l_{j,t}) = \mathbb{E}(q_{j,t}) \mathbb{E}(l_{j,t}) \quad (8)$$

$$\frac{1}{m} \sum_{\forall t} \sum_{j=1}^m q_{j,t} l_{j,t} = \sum_{\forall t} \left( \frac{1}{m} \sum_{j=1}^m q_{j,t} \right) \frac{1}{m} \sum_{\forall t} \sum_{j=1}^m l_{j,t} \quad (9)$$

$$\sum_{\forall j,t} q_{j,t} l_{j,t} = \sum_{\forall t} (\bar{q}_{eq,t}) \sum_{\forall j,t} l_{j,t} \quad (10)$$

Similarly, for non-equipped networks:

$$\sum_{\forall t} TTD_{neq,t} = \sum_{\forall i \in \{neq\}} q_{i,t} l_{i,t} \quad (11)$$

$$\mathbb{E}(q_{i,t} l_{i,t} | \forall i \notin j, t) = \mathbb{E}(q_{i,t} | \forall i \notin j, t) \mathbb{E}(l_{i,t} | \forall i \notin j, t) \quad (12)$$

$$\sum_{\forall t} \sum_{i=1}^p q_{i,t} l_{i,t} = \sum_{\forall t} (\bar{q}_{neq,t}) \sum_{\forall t} \sum_{i=1}^p l_{i,t} \quad (13)$$

$$\sum_{\forall i \notin j, t} q_{i,t} l_{i,t} = \sum_{\forall t} (\bar{q}_{neq,t}) \sum_{\forall i \notin j, t} l_{i,t} \quad (14)$$

Assuming the mean flow for a non-equipped network is the same as an equipped network for a unique hierarchy, i.e.,  $(\bar{q}_{neq,t} = \bar{q}_{eq,t})$ . Therefore, by applying (10) to (14), we get the following estimation of TTD for a non-equipped network.

$$\sum_{\forall i \notin j, t} q_{i,t} l_{i,t} = \frac{\sum_{\forall j, t} q_{j,t} l_{j,t}}{\sum_{\forall j, t} l_{j,t}} \sum_{\forall i \notin j, t} l_{i,t} \quad (15)$$

$$= \sum_{\forall j, t} q_{j,t} l_{j,t} \frac{\sum_{\forall i \notin j, t} l_{i,t}}{\sum_{\forall j, t} l_{j,t}} \quad (16)$$

Thus, the total network flow can be estimated from the equipped network information as follows:

$$\hat{q} = \frac{\sum_{\forall t} TTD}{\sum_{\forall i, t} l_{i,t} \Delta t} \quad (17)$$

$$= \frac{\sum_{\forall t} TTD_{eq} + \sum_{\forall t} TTD_{neq}}{\sum_{\forall i, t} l_{i,t} \Delta t} \quad (18)$$

$$= \frac{\sum_{\forall j, t} q_{j,t} l_{j,t} + (\sum_{\forall j, t} q_{j,t} l_{j,t} \frac{\sum_{\forall i \notin j, t} l_{i,t}}{\sum_{\forall j, t} l_{j,t}})}{\sum_{\forall i, t} l_{i,t} \Delta t} \quad (19)$$

Similarly, we can also derive the network average density from the equipped network. The network average density can be expressed by total travel time (TTT) as the ‘accumulation’ spent by all vehicles in the network over the time-space domain. Similar to the TTD in (2), we can estimate TTT in the equipped network as  $TTT_{eq} = \sum_{\forall j} k_j l_j$ . Local densities at LD-level ( $k_j$ ) need to be corrected since the LDs suffer from location-biased and systematic errors. This study corrected LD-level density estimation as per the methods mentioned in Maiti (2024). Therefore, the total network density can be formulated from the

corrected LD in the equipped network as follows:

$$\hat{k} = \frac{\sum_{\forall t} TTT}{\sum_{\forall i,t} l_{i,t} \Delta t} \quad (20)$$

$$= \frac{\sum_{\forall t} TTT_{eq} + \sum_{\forall t} TTT_{neq}}{\sum_{\forall i,t} l_{i,t} \Delta t} \quad (21)$$

$$= \frac{\sum_{\forall j,t} k_{j,t} l_{j,t} + (\sum_{\forall j,t} k_{j,t} l_{j,t} \frac{\sum_{\forall i \notin j,t} l_{i,t}}{\sum_{\forall j,t} l_{j,t}})}{\sum_{\forall i,t} l_{i,t} \Delta t} \quad (22)$$

The variables  $q_{j,t}$  and  $k_{j,t}$  represent flow and density in the equipped network of  $t$  link hierarchy, estimated at the detector level on a link.

## 2.2. Spatial Imputation: Variogram

Instead of scaling observations from the equipped network to represent the non-equipped network, an alternative approach is to impute flow and density values for all links and subsequently calculate the full MFD. To achieve this, we propose using a spatial variogram-based method for the imputation process. Kriging is a well-established geostatistical interpolation method initially developed by [Krige \(1951\)](#) and later expanded by [Matheron \(1963\)](#). It has been applied across various disciplines for spatial data interpolation, including missing data imputation in traffic studies. The central component of kriging is the variogram, a function that models the spatial correlation between data points. The variogram provides an essential representation of how spatial dependence changes with distance, guiding Kriging's ability to estimate unknown values at unobserved locations based on nearby known observations ([Cressie, 1993](#)).

Variogram models, such as spherical, exponential, and Gaussian models, are typically fitted to the empirical variogram to quantify spatial continuity ([Oliver, 2014](#)). These models help define the structure of spatial relationships and enable kriging to make predictions.

### 2.2.1. Spatial Dependency and Variogram

Let the traffic flow data for certain links in a network be given as  $\{(s_i, q_i)\}$ , where  $s_i = (x_i, y_i)$  represents the geographical coordinates (latitude and longitude) of the  $i$ -th known link, and  $q_i$  is the observed traffic flow at that link. The task is to estimate traffic flow  $q(s_0)$  at unknown locations  $s_0$  by leveraging spatial interpolation techniques based on a variogram-based model.

The variogram measures the spatial dependence of a random variable, in this case, traffic flow, across a network. The variogram  $\gamma(h)$  represents how traffic flow differences are expected to change with increasing distance ( $h$ ) between two locations. Unlike the traditional variogram model's spatial distance, in this study, the distance between two locations is measured by the shortest path distance along the road network. For any two points  $s_i$  and  $s_j$  separated by

distance  $h = \|s_i - s_j\|$ , the variogram is defined as:

$$\gamma(h) = \frac{1}{2} \mathbb{E} [(q(s_i) - q(s_j))^2] \quad (23)$$

Here,  $\mathbb{E}$  denotes the expectation, and  $h$  is the shortest path distance between  $s_i$  and  $s_j$ .

The variogram is often approximated from data using the empirical variogram:

$$\gamma(h) = \frac{1}{2N(h)} \sum_{s_i, s_j: \|s_i - s_j\|=h} (q_i - q_j)^2 \quad (24)$$

where  $N(h)$  is the number of pairs of points separated by distance  $h$ . This empirical variogram helps identify the spatial structure in the traffic flow data. The variogram  $\gamma(h)$  is typically modeled using one of several functional forms (e.g., spherical, exponential, Gaussian) based on the empirical semivariances derived from the data. For instance, the spherical variogram is expressed as:

$$\gamma(r) = \begin{cases} C_0 + C \left( \frac{3r}{2a} - \frac{r^3}{2a^3} \right), & \text{if } r \leq a \\ C_0 + C, & \text{if } r > a \end{cases} \quad (25)$$

where  $a$  is the range,  $C_0$  is the nugget, and  $C$  is the sill, serve as constants for the model.

### 2.2.2. Spatial Interpolation: Kriging System Setup

Once the variogram model is fitted, the traffic flow at unmeasured locations can be estimated using *Ordinary Kriging*. In Ordinary Kriging (OK) for traffic flow estimation, we aim to predict the traffic flow  $\hat{q}(s_0)$  at an unmeasured location  $s_0$ , using a weighted linear combination of the traffic flows  $q(s_i)$  at known locations  $s_i$ , where  $i = 1, 2, \dots, n$ . The primary assumption in OK is that the mean traffic flow  $\bar{q}(s)$  is constant within a neighborhood of the target point  $s_0$ . The following assumptions are considered:

- The deterministic component  $\bar{q}(s)$ , representing the mean traffic flow, is approximately constant across the neighborhood of interest, so  $\bar{q}(s_0) \approx \bar{q}(s_i) \equiv \bar{q}$ .
- The stochastic component  $\epsilon(s)$ , representing random fluctuations in traffic flow, is Gaussian-distributed with zero mean, and the correlation between flows at different locations depends on their spatial separation.

The predicted traffic flow  $\hat{q}(s_0)$  at location  $s_0$  is given by:

$$\hat{q}(s_0) = \bar{q}(s_0) + \epsilon(s_0) \quad (26)$$

The random component can be defined as a weighted multiplication of the deviation of the observed traffic flow at  $s_i$  from the mean  $s_0$ . The kriging weights  $w_i$  are applied to these deviations, meaning that locations closer to  $s_0$  (with



higher spatial correlation) will have a greater influence on the prediction. This spatially weighted adjustment ensures that the predicted traffic flow at  $s_0$  not only considers the global mean  $\bar{q}$  but also incorporates the local variations (the deviations from the mean) based on the observed traffic flows at the nearby locations.

$$\hat{q}(s_0) = \bar{q} + \sum_{i=1}^n w_i (q(s_i) - \bar{q}) \quad (27)$$

Since  $\bar{q}$  is assumed to be constant, the estimator simplifies to:

$$\hat{q}(s_0) = \sum_{i=1}^n w_i q(s_i) + \bar{q} \left( 1 - \sum_{i=1}^n w_i \right) \quad (28)$$

For an unbiased estimator, the weights  $w_i$  must satisfy the constraint:

$$\sum_{i=1}^n w_i = 1 \quad (29)$$

Therefore, the predicted traffic flow at  $s_0$  is given by:

$$\hat{q}(s_0) = \sum_{i=1}^n w_i q(s_i) \quad (30)$$

The expected value of the predicted traffic flow is equal to the expected value of the true traffic flow:

$$\mathbb{E}[\hat{q}(s_0)] = \bar{q} = \mathbb{E}[q(s_0)] \quad (31)$$

The kriging weights  $w_i$  are determined by solving the kriging system of  $n + 1$  equations for the weights  $w_i$  and Lagrange multiplier  $\mu$  is:

$$\begin{pmatrix} \gamma_{11} & \gamma_{12} & \dots & \gamma_{1n} & 1 \\ \gamma_{21} & \gamma_{22} & \dots & \gamma_{2n} & 1 \\ \vdots & \vdots & \ddots & \vdots & \vdots \\ \gamma_{n1} & \gamma_{n2} & \dots & \gamma_{nn} & 1 \\ 1 & 1 & \dots & 1 & 0 \end{pmatrix} \begin{pmatrix} w_1 \\ w_2 \\ \vdots \\ w_n \\ \mu \end{pmatrix} = \begin{pmatrix} \gamma_{10} \\ \gamma_{20} \\ \vdots \\ \gamma_{n0} \\ 1 \end{pmatrix} \quad (32)$$

Where  $\gamma_{ij}$  is the semivariance between known points  $s_i$  and  $s_j$ ,  $\gamma_{i0}$  represents the semivariance between  $s_i$  and  $s_0$ .

### 3. Data

This section describes the empirical data used in this study, focusing on LDD collected under varying levels of sensor deployment. Additionally, it outlines the link hierarchy classification, which forms the basis for the hierarchical scaling methodology proposed in this study.

### 3.1. Data Description

The study focuses on the road network of downtown Athens, Greece, covering an area of approximately 40 km<sup>2</sup>. The network, excluding minor roads, extends over 150 km in total length. The major roads, characterized by more than two lanes and a peak-hour traffic flow exceeding 1000 vehicles per lane per hour, are identified as the most important and busiest routes within the network. The data for this study was collected from loop detectors over a weekday period from November 7th to 11th, 2022, covering a 24-hour time span each day. The loop detector data provides location-based traffic information, such as traffic counts and average speeds.

The links in the road network were classified in two ways. The first classification follows a three-hierarchy (3-H), where roads are categorized into three groups: Link-1, corresponding to the most critical roads, and Link-3, the least important major roads. The second classification follows a two-tier hierarchy (2-H), where the network is divided into two types: Link-1, representing the most important roads, and Link-2, which includes the remaining major roads. Notably, Link-1 is identical in both classifications, while Link-2 in the 2-H classification corresponds to Link-2 and Link-3 in the 3-H classification based on their average speeds and flow profiles. No additional link classes beyond the 3-H level were identified as exhibiting statistically significant differences in traffic and road characteristics. This link hierarchy is Figures 2 and 3 illustrate the comparison of average speeds and flow profiles for the 2-H and 3-H classifications. We can see in Figure 3 that the average speed and flow in each group are significantly different, so using a common flow average from the equipped network to estimate the average flow on the non-equipped network leads to strong bias.

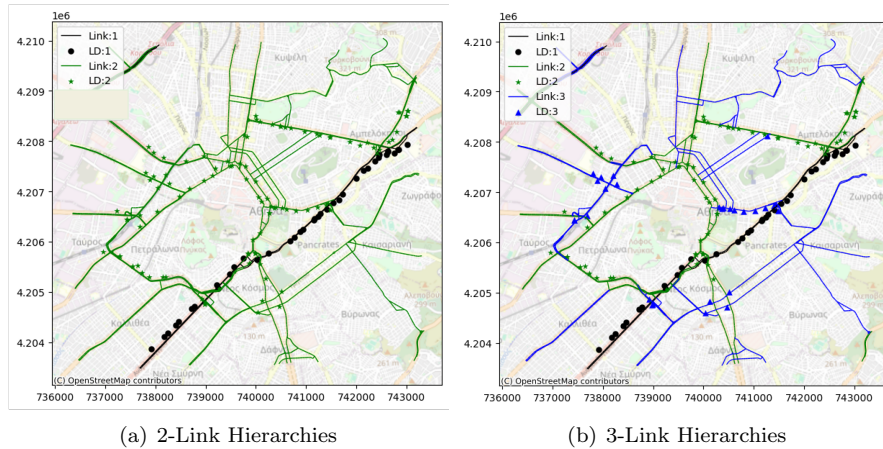


Figure 2: Network fully equipped with LDD and features hierarchical links, including (a) two types link, (b) three types link

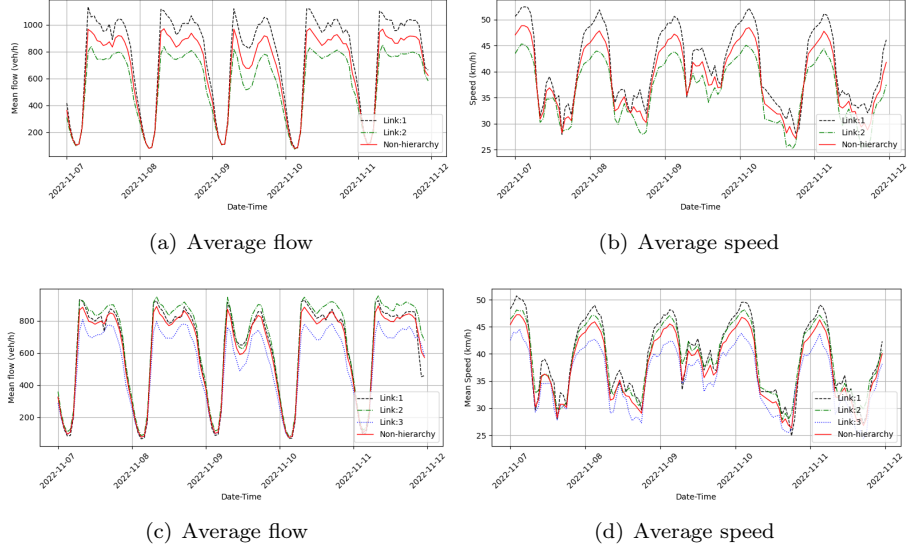


Figure 3: Comparison of average network flow ((a) two-hierarchy, (c) three-hierarchy) and speed ((b) two-hierarchy, (d) three-hierarchy) for different network configurations.

The study focuses on a road network comprising 2,456 links, spanning various hierarchical levels within a 150 km area. A fully equipped network is defined as one where every link is equipped with at least one LD. However, only 142 of these links currently have LDs installed. Therefore, the LDs percentage in the network is approximately 5.78%. To address this limitation, a partially equipped network was constructed, utilizing the data from these 142 links to estimate MFDs for validation purposes. For comparison, the fully equipped network was conceptualized as including the 142 LDs distributed across their respective links, as illustrated in Figures 2 (a, b). To evaluate our methodology, we also created partially equipped networks by randomly removing LDs from various links equally from each hierarchy in both the 2-H and 3-H hierarchical networks. Table 1 provides details on the number of LDs in each link type for the fully equipped (100%) network as well as for networks with 30%, 20%, 10%, and 5% LD coverage. Figure 4 illustrates the distribution of LDs in these partially equipped networks.

In this study, the proposed approach was validated using two distinct network types: the 2-H network, the 3-H network, and a baseline non-hierarchical network for comparison.

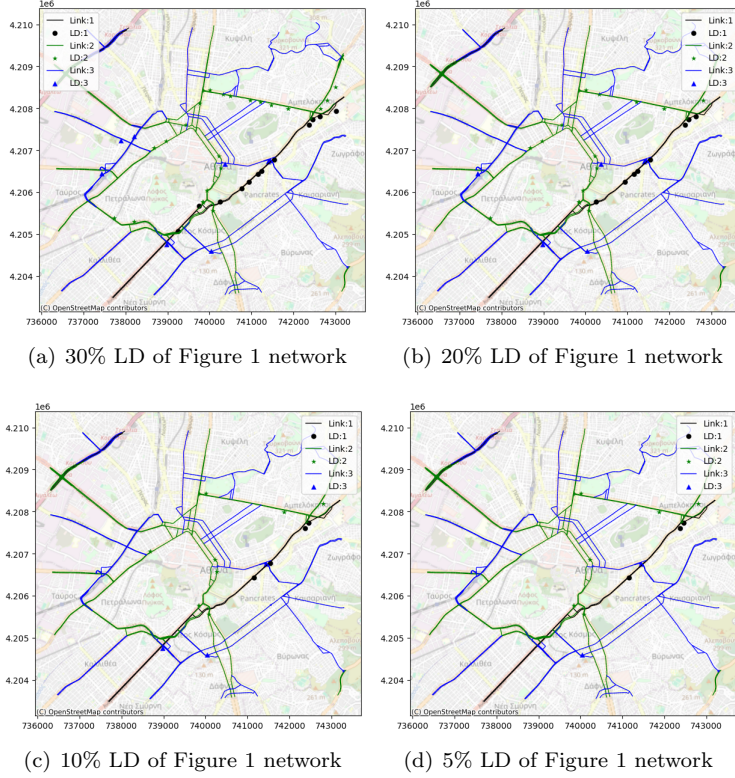


Figure 4: Partially loop detectors equipped networks (a) 30% LD equipped network, (b) 20% LD equipped network, (c) 10% LD equipped network, and (d) 5 % LD equipped network

Table 1: Description of loop detector-equipped link in the fully equipped and partially equipped network

Equipped Network (% LD)	3-Hierarchies			2-Hierarchies		Non-Hierarchy
	Link-1	Link-2	Link-3	Link-1	Link-2	Link-all
100	39 (20 km)	75 (60 km)	28 (70 km)	45 (20 km)	95 (130 km)	142 (150 km)
30	12	22	8	16	26	42
20	8	15	6	10	19	29
10	4	8	3	6	9	15
5	2	4	1	3	4	7

## 4. Results

The study proposes two methods: first, hierarchical scaling with application to the 2-H and 3-H network approach. Second, the spatial data imputation with the variogram method to spatially interpolate the network variables in the full network. In the end, we compared the estimated network variables and MFDs with the baseline non-hierarchical network approach.

### 4.1. Flow estimation using spatial imputation methods: variogram

The Variogram model takes input of flow from the equipped network’s links and estimates flow spatially over the full network. Figure 5 demonstrates the flow estimation spatially with respect to different percentages of LD-equipped networks at various times of the day. The color-coded flow plots visually represent traffic flow intensity across the network links, with the gradient indicating varying flow levels, from low (blue) to high (red). Since this study focuses on flow scaling only on the major roads (Link-1, link-2, link-3), we only extracted information along the links in the major roads. In the first column of Figure 5, where 30% of the network’s major links are equipped with loop detectors (LD), the Variogram model produces a detailed and accurate estimation of flow across all major and minor links. Congestion hotspots, as indicated by red zones, align closely with expected traffic patterns, validating the model’s capability to capture traffic dynamics effectively under sufficient LD coverage. As the LD percentage is reduced to 20% and 10%, shown in the subsequent columns, the model maintains a good estimation quality of the overall network flow, with significant flow details retained for major road links (Link-1, Link-2, and Link-3). Congestion hotspots and the broader distribution of flow are generally well-captured, indicating the robustness of the Variogram-based estimation even under reduced LD coverage.

As we further decrease the LD percentage to 5%, this method was not able to estimate full network traffic flow because of the sparse information with respect to the variogram radius of estimation. Therefore, this method is best suited for network flow scaling of an equipped network having more than 10 % LD. However, at the 5% LD level (final column), the model’s performance declines. Sparse detector data creates spatial gaps that hinder accurate network flow estimation. This results in less precise representations of flow across the network, with notable discrepancies in congestion hotspots and overall flow intensity. This limitation highlights the importance of maintaining a critical mass of LD coverage for accurate spatial flow estimation. Our goal is not to determine the flow on links but to perform imputation in a way that ensures accurate aggregation when calculating the network’s average flow.

Across all LD percentages, flow estimations vary consistently throughout the day (from 08:00 to 17:00). Peak traffic hours show distinct congestion patterns, emphasizing the model’s sensitivity to temporal variations in traffic demand and conditions. The consistent ability of the Variogram model to capture these temporal patterns, even as LD coverage changes, is a notable strength. This analysis underscores that the Variogram-based method for network flow scaling

performs optimally with LD coverage of at least 10%. Below this threshold, estimation accuracy declines significantly due to sparse spatial data, reducing the reliability of flow predictions.

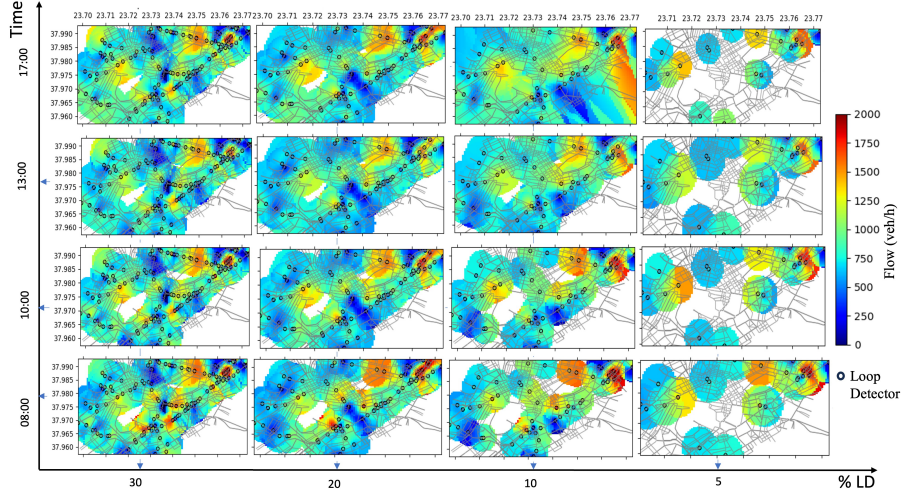


Figure 5: Traffic flow prediction from the equipped network to the entire network using the Variogram method. The x-axis represents the equipped network with varying LD percentages, while the y-axis depicts traffic flow at different hours of the day at both the LD position and network level.

#### 4.2. Comparison of proposed methods

The results presented in Figures 6 and 7, along with the RMSE values in Table 2, provide a detailed comparison of the proposed hierarchical network scaling method, the variogram-based approach, and the baseline non-hierarchical network scaling. This evaluation focuses on their performance in estimating network flow under different levels of LD coverage, specifically at 5%, 10%, 20%, and 30%. The temporal flow estimations in Figure 6 show that the baseline (non-hierarchical) quickly loses accuracy when the LD coverage is reduced below 20%. It results in an inaccurate estimation of network flow, causing significant bias in the MFD. Recall the usual network with 5.78 % LDs coverage, which is very low and far from 20% LDs coverage. At the lowest LD coverage (5%), the Variogram method is unable to estimate flow across the entire network, reflecting a limitation in this approach when LD coverage falls below 10%. At 10% LD coverage, the Variogram method becomes viable and achieves relatively low RMSE values compared to non-hierarchical network scaling. Although the variogram method with 10% and 20% LD coverage demonstrates improved accuracy compared to the baseline, it also results in greater fluctuations in higher flow regimes (see Figure 6). Meanwhile, the hierarchical network scaling performs better in the low coverage of LD with minimum deviation and fluctuation compared to the

actual flow. In the hierarchical method, the 3-H network cluster demonstrates best among the overall methodologies. The 3-Hierarchy continues to provide estimations, though with elevated RMSE values (e.g., RMSE of 65-64 on day 1 and day 4 for the 3-Hierarchy method). This highlights the robustness of hierarchical frameworks compared to geospatial imputation techniques like the Variogram, which require a minimum density of LDs for effective network-wide prediction compared to the non-hierarchical scaling approach. Across all methods, higher LD coverage consistently leads to more accurate predictions. RMSE values significantly decrease once LD coverage reaches 20%-30%, a benchmark that is challenging to achieve in practice. The average RMSE for five days of network traffic flow estimation at LD coverage of 10% is 29.2 vehicles per hour (veh/h) using the 3-H approach, compared to 41.6 veh/h with the variogram method. When the LD coverage decreases to 5%, the RMSE for the 3-H method increases to 56 veh/h, which remains a reasonable estimation given the reduced coverage of LDs. In the hierarchical network methods, increasing the number of hierarchy groups in the network consistently enhances estimation accuracy. Therefore, at any given LD coverage percentage, the 3-hierarchy (3-H) network consistently outperforms the baseline and other methods.

The scatter plots in Figure 7 further illustrate these trends, showing the spread of estimated flow values relative to actual flow values from a fully equipped network. As LD coverage decreases, the spread around the ideal  $x = y$  line widens, particularly for the non-hierarchical method, which exhibits greater deviations from actual values. Conversely, the 3-Hierarchy and variogram approaches demonstrate tighter clustering around the ideal line, especially at lower LD coverages, reaffirming their superior accuracy under moderate to high LD densities.

These results underscore the robustness of hierarchical network scaling, particularly in sparse LD conditions where unstructured methods like the Variogram may falter. The 3-H method, in particular, shows resilience across all coverage levels, while the Variogram method performs strongly at 10% and higher LD coverage, demonstrating its potential for accurate network-wide estimations when sufficient spatial data is available. The baseline approach, applied under the lower usual case of 5% LD coverage, yields a network-average flow estimation with an RMSE of 234 veh/h. This value is notably four times higher than the error achieved using the proposed three-level hierarchical (3-H) network scaling method. These findings underscore the importance of adopting a hierarchical network approach to improve the accuracy of traffic variable estimation at the network level.



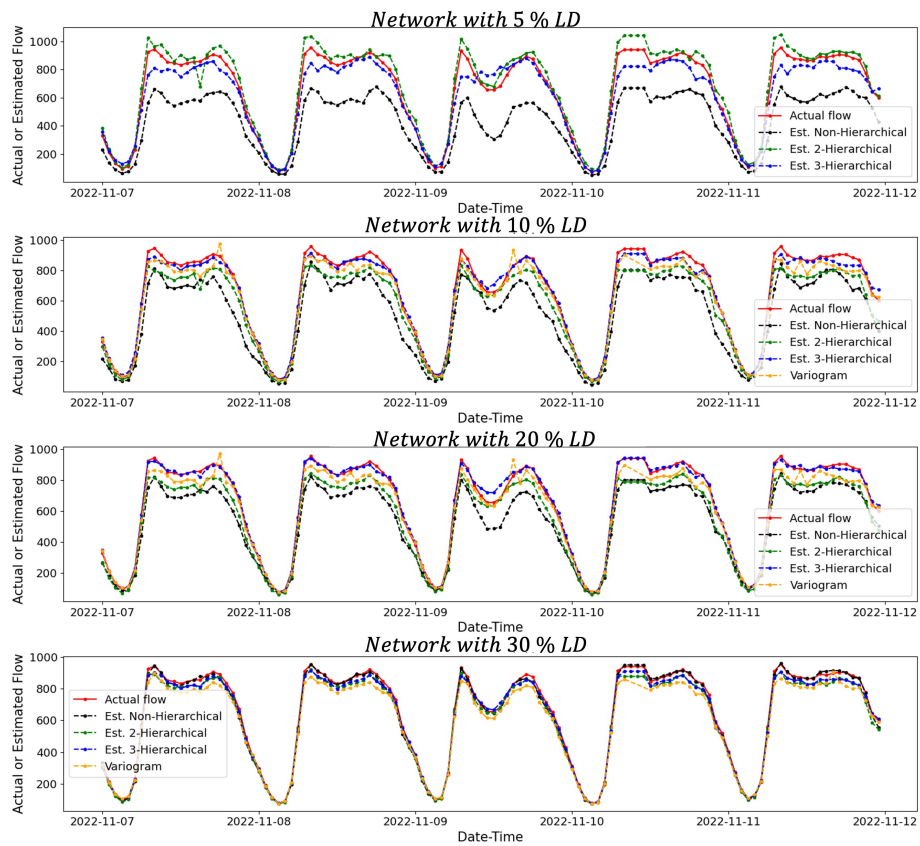


Figure 6: Comparisons of estimated hourly network flow using different methods with different loop detector equipped network level.

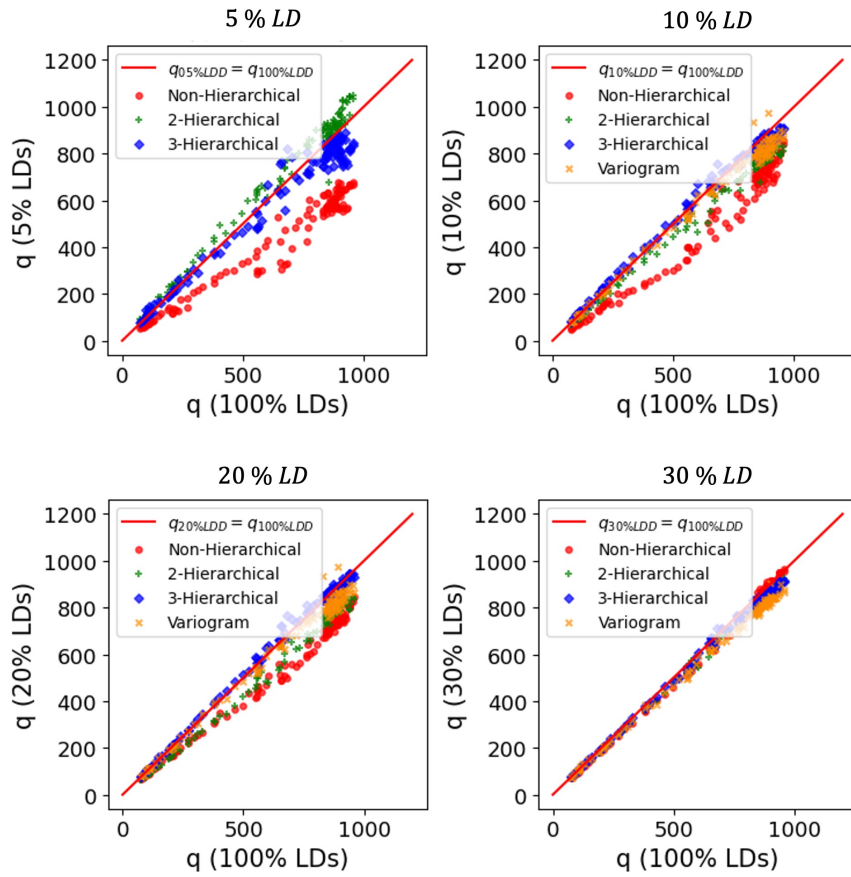


Figure 7: Comparison of actual network flow based on fully equipped network information (100% LD) with estimated flow derived from a partially equipped network. The x-axis represents the actual flow, while the y-axis denotes the estimated flow. From left to right, the subfigures illustrate comparisons for 5%, 10%, 20%, and 30% LD.

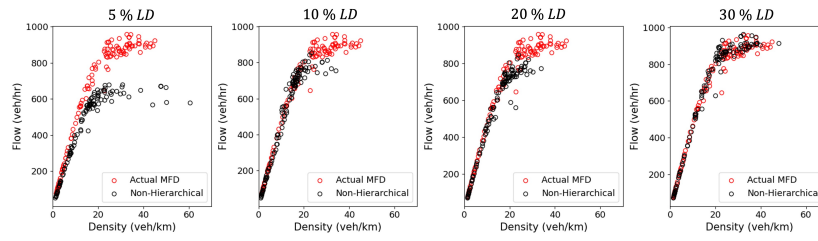
Table 2: Comparison of root mean square error (RMSE) of network flow, estimated using different network scaling methods

Day	Network (% LD)	3-H	2-H	Non-hierarchy	Variogram
day1	30	<b>12</b>	30	24	12
	20	<b>12</b>	85	128	17
	10	<b>26</b>	90	158	43
	5	<b>65</b>	110	226	-
day2	30	<b>13</b>	29	20	15
	20	<b>14</b>	83	127	29
	10	<b>26</b>	87	148	45
	5	<b>53</b>	108	232	-
day3	30	<b>25</b>	24	20	42
	20	<b>27</b>	70	133	27
	10	<b>28</b>	83	142	42
	5	<b>51</b>	120	260	-
day4	30	<b>12</b>	37	17	25
	20	<b>13</b>	94	119	15
	10	<b>31</b>	98	144	39
	5	<b>64</b>	117	224	-
day5	30	<b>13</b>	42	16	31
	20	<b>16</b>	94	110	34
	10	<b>35</b>	95	145	39
	5	<b>48</b>	115	229	-

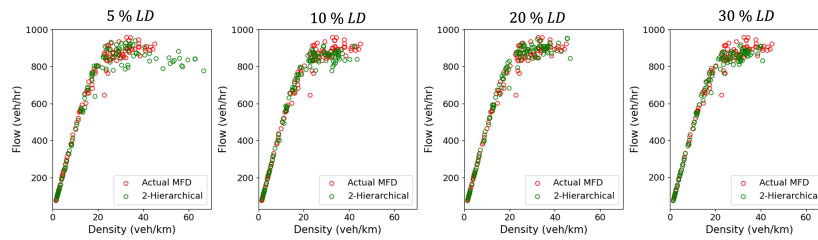
### 4.3. Comparing MFDs

This section demonstrates network MFDs estimated from the partially equipped network using the proposed scaling methodologies and compares them with the actual MFDs from the fully equipped network. In section 2.1, we proposed the network flow ( $\hat{q}$ ) and density ( $\hat{k}$ ) using the hierarchical scaling method, and section 2.2 described  $\hat{q}$  estimation using the variogram. Similarly, we can estimate  $\hat{k}$  using variogram methods by estimating detector-level density.

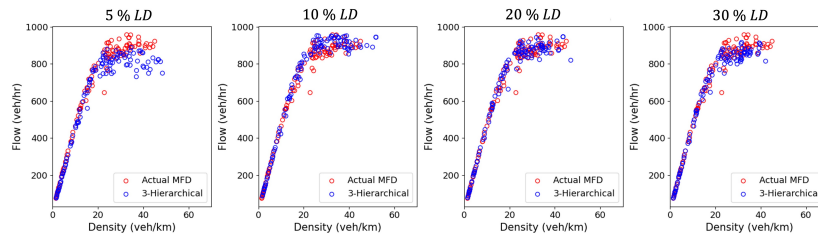
The estimated MFDs derived from the proposed methodologies across varying LD coverage percentages demonstrate clear differences in accuracy among the methods employed, as summarized in Figure 8 and Table 3. The 5% LD scenario represents the most challenging condition for MFD estimation due to sparse detector data. Among the methods, the three-hierarchy (3-H) statistical scaling achieves the lowest RMSE of 48.9 veh/h, significantly outperforming the two-hierarchy (2-H) scaling (51.8 veh/h) and the non-hierarchical approach (175.5 veh/h). The high coefficient of determination ( $R^2 = 0.97$ ) for the 3-H method further highlights its robustness in low-data scenarios, maintaining strong alignment with the actual MFD. For 10% LD, the 3-H scaling method again delivers superior results with an RMSE of 45.3 veh/h, slightly better than the 2-H method (45.7 veh/h), variogram (55.2 veh/h), and markedly better than the non-hierarchical approach (137.6 veh/h). At 20% LD, the differences between the hierarchical methods narrow further, with 3-H achieving 36.5 veh/h RMSE compared to 37.3 veh/h for 2-H. Both methods significantly outperform the non-hierarchical method (133.5 veh/h), demonstrating the effectiveness of incorporating spatial structure in flow estimation. At the highest detector coverage of 30%, all methods perform well due to the availability of more extensive data.



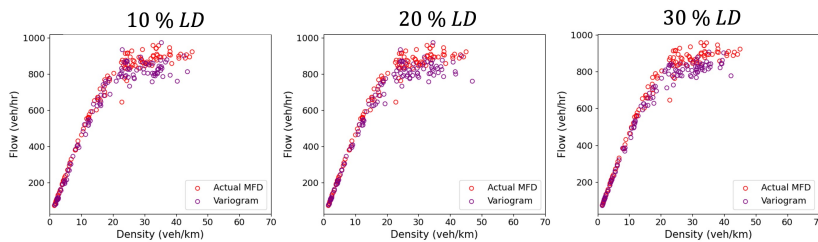
(a) Statistical scaling in non-hierarchical network



(b) Statistical scaling in two-hierarchical network



(c) Statistical scaling in three-hierarchical network



(d) Variogram scaling in non-hierarchical network

Figure 8: Comparison of estimated MFDs from partially equipped networks: (a, b, c) represent 5%, 10%, 20%, and 30% LD from left to right, and (d) shows 10%, 20%, and 30% LD from left to right, compared with the actual MFD derived from a fully equipped (100% LD) network.

Table 3: Comparison of estimated and actual MFDs

Method	Network Types	% LD	RMSE (veh/h)	$R^2$
Statistical	Non-hierarchy	30	39.9	0.98
		20	133.5	0.79
		10	137.6	0.78
		5	175.5	0.64
	Three-hierarchy	30	<b>35.9</b>	0.98
		20	<b>36.5</b>	0.98
		10	<b>45.3</b>	0.97
		5	<b>48.9</b>	0.97
	Two-hierarchy	30	37.1	0.98
		20	37.3	0.98
		10	45.7	0.97
		5	51.8	0.96
Variogram	Non-hierarchy	30	51.5	0.97
		20	54.6	0.96
		10	55.2	0.96

Using the hierarchical network clustering methods, we estimate the full network MFD, as illustrated in Figure 9, and compare these results with the baseline method. The full network consists of all 2456 links as described in data description section. It is evident from the figure that the baseline method underestimates the MFD, particularly in the critical density regime. However, in the free-flow regime, both approaches yield comparable results. Recalling the network LD coverage as 5.68%, we can refer to the MFDs in Figure 8 (a) for 5% LD; the same pattern is observed here. To simplify our analysis, we fitted the scattered MFDs using a non-linear model and created 95% confidence intervals. The best-fit three-hierarchy model can estimate about 66 veh/h more in the critical density regime, along with a slight improvement in the maximum observed network density. Although it is not too significant for our case, for a larger and more hierarchical network, it may significantly impact the MFD estimation. While the limited LD coverage poses challenges for validating the full network MFD, the hierarchical scaling approach demonstrates a significant improvement over the baseline method, particularly in capturing the critical density region.

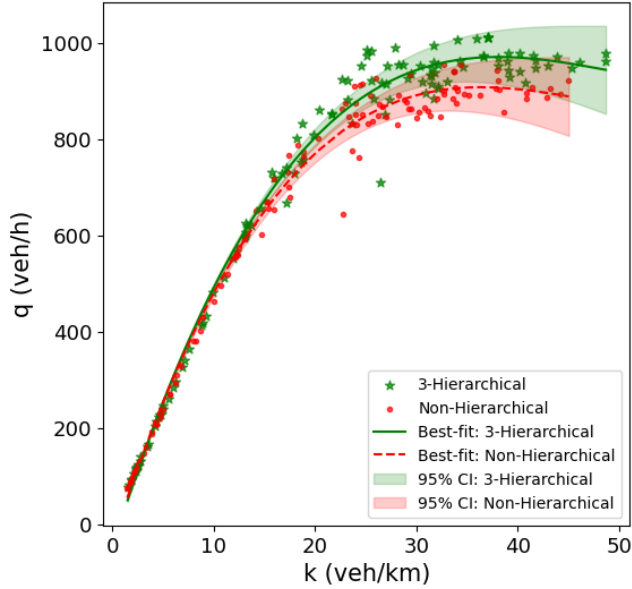


Figure 9: Comparing the estimated MFD using a hierarchical network cluster with three hierarchies to the baseline non-hierarchical method for the entire network consisting of 2456 links.

## 5. Conclusion

This study presents a novel methodology for estimating network-wide traffic characteristics in partially sensor-equipped urban networks. By integrating hierarchical network scaling and geospatial imputation techniques, the framework provides accurate estimations of MFDs, even in networks with sparse detector coverage. The results underscore the critical role of hierarchical scaling in improving network traffic variables and MFD estimation accuracy, particularly under sparse data conditions. The 3-H method consistently outperforms (lowest RMSE and highest  $R^2$  values) the 2-H and variogram approaches across all LD levels, with its advantage most pronounced at low LD coverage (5% and 10%). This is likely due to the additional spatial structure incorporated in the hierarchical scaling, which allows it to better capture localized variations in flow and density. Also, we found that more number of network hierarchies influence better estimation of network traffic states and MFDs. The estimation of the full network's MFD using three hierarchical network clusters reveals significant deviations in network saturation flow and critical density range compared to traditional methods, as illustrated in Figure 9. The baseline scaling method shows improved accuracy as more data becomes available, but it remains less reliable than its hierarchical counterparts due to its inability to effectively extrapolate flow patterns in under-monitored regions. Interestingly, the variogram approach demonstrates competitive performance for LD coverage levels of 10% or more



with small fluctuations in high flow regimes, but it was incompetent at lower (5%) LD due to insufficient data for spatial imputation. This limitation highlights the trade-offs between different methods in terms of data requirements and estimation capabilities. As a geospatial interpolation tool, the variogram model estimates non-equipped link variables based on spatial distribution. Although route distances between links were used instead of Euclidean spatial distances, some interpolation errors may arise, affecting accuracy. In contrast, the hierarchical method is more promising because it assumes that links within the same hierarchy exhibit similar mean and covariance properties. It offers a scalable and practical solution for estimating network-wide traffic conditions under varying levels of sensor availability. The findings underscore the potential of incorporating network structure and spatial dependencies in traffic modeling for real-world applications. Therefore, this study bridges the gap between partial sensor data and full-network traffic estimation for cities with limited sensor coverage. Overall, the findings emphasize the importance of leveraging network hierarchical frameworks for MFD estimation, particularly in scenarios where data availability is limited. The superior performance of the 3-H method highlights its potential for practical applications in network flow analysis, even under challenging conditions.

### **Acknowledgement**

This research has received funding from the European Union’s Horizon Europe research and innovation program under Grant Agreement no. 101103808 (ACUMEN). The authors would like to thank Prof. Eleni I. Vlahogianni and her team from NTUA Athens for their support in providing traffic data.

## References

- C. F. Daganzo, N. Geroliminis, An analytical approximation for the macroscopic fundamental diagram of urban traffic, *Transportation Research Part B: Methodological* 42 (2008) 771–781. doi:[10.1016/j.trb.2008.06.008](https://doi.org/10.1016/j.trb.2008.06.008).
- M. Keyvan-Ekbatani, M. Yildirimoglu, N. Geroliminis, M. Papageorgiou, Multiple concentric gating traffic control in large-scale urban networks, *IEEE Transactions on Intelligent Transportation Systems* 16 (2015) 2141–2154. doi:[10.1109/TITS.2015.2399303](https://doi.org/10.1109/TITS.2015.2399303).
- K. Ampountolas, N. Zheng, N. Geroliminis, Macroscopic modelling and robust control of bi-modal multi-region urban road networks, *Transportation Research Part B: Methodological* 104 (2017) 616–637. doi:[10.1016/j.trb.2017.05.007](https://doi.org/10.1016/j.trb.2017.05.007).
- K. Aboudolas, N. Geroliminis, Perimeter and boundary flow control in multi-reservoir heterogeneous networks, *Transportation Research Part B: Methodological* 55 (2013) 265–281. doi:[10.1016/j.trb.2013.07.003](https://doi.org/10.1016/j.trb.2013.07.003).
- G. Mariotte, L. Leclercq, Heterogeneous perimeter flow distributions and MFD-based traffic simulation, *Transportmetrica B* 7 (2019) 1378–1401. doi:[10.1080/21680566.2019.1627954](https://doi.org/10.1080/21680566.2019.1627954).
- S. Jiang, M. Keyvan-Ekbatani, Hybrid perimeter control with real-time partitions in heterogeneous urban networks: An integration of deep learning and MPC, *Transportation Research Part C: Emerging Technologies* 154 (2023). doi:[10.1016/j.trc.2023.104240](https://doi.org/10.1016/j.trc.2023.104240).
- C. Buisson, C. Ladier, Exploring the impact of homogeneity of traffic measurements on the existence of macroscopic fundamental diagrams, *Transportation Research Record* (2009) 127–136. doi:[10.3141/2124-12](https://doi.org/10.3141/2124-12).
- N. Geroliminis, J. Sun, Hysteresis phenomena of a macroscopic fundamental diagram in freeway networks, in: *Procedia - Social and Behavioral Sciences*, volume 17, Elsevier Ltd, 2011, pp. 213–228. doi:[10.1016/j.sbspro.2011.04.515](https://doi.org/10.1016/j.sbspro.2011.04.515).
- M. Keyvan-Ekbatani, A. Kouvelas, I. Papamichail, M. Papageorgiou, Exploiting the fundamental diagram of urban networks for feedback-based gating, *Transportation Research Part B: Methodological* 46 (2012) 1393–1403. doi:[10.1016/j.trb.2012.06.008](https://doi.org/10.1016/j.trb.2012.06.008).
- M. Saberi, H. Mahmassani, Exploring properties of networkwide flow-density relations in a freeway network, *Transportation Research Record* (2012) 153–163. doi:[10.3141/2315-16](https://doi.org/10.3141/2315-16).
- M. Keyvan-Ekbatani, M. Papageorgiou, I. Papamichail, Urban congestion gating control based on reduced operational network fundamental diagrams, *Transportation Research Part C: Emerging Technologies* 33 (2013) 74–87. doi:[10.1016/j.trc.2013.04.010](https://doi.org/10.1016/j.trc.2013.04.010).

- L. Ambühl, A. Loder, L. Leclercq, M. Menendez, Disentangling the city traffic rhythms: A longitudinal analysis of MFD patterns over a year, *Transportation Research Part C: Emerging Technologies* 126 (2021). doi:[10.1016/j.trc.2021.103065](https://doi.org/10.1016/j.trc.2021.103065).
- G. Lee, Z. Ding, J. Laval, Effects of loop detector position on the macroscopic fundamental diagram, *Transportation Research Part C: Emerging Technologies* 154 (2023). doi:[10.1016/j.trc.2023.104239](https://doi.org/10.1016/j.trc.2023.104239).
- O. Mousavizadeh, M. Keyvan-Ekbatani, On the important features for a well-shaped reduced network MFD estimation during network loading and recovery, *Transportation Research Part C: Emerging Technologies* 161 (2024). doi:[10.1016/j.trc.2024.104539](https://doi.org/10.1016/j.trc.2024.104539).
- L. Leclercq, N. Chiabaut, B. Trinquier, Macroscopic Fundamental Diagrams: A cross-comparison of estimation methods, *Transportation Research Part B: Methodological* 62 (2014) 1–12. URL: <http://dx.doi.org/10.1016/j.trb.2014.01.007>. doi:[10.1016/j.trb.2014.01.007](https://doi.org/10.1016/j.trb.2014.01.007).
- L. Maiti, Nandan; Leclercq, Correcting Loop Detector Positional Bias When Estimating Macroscopic Fundamental Diagrams Using Link Speed Data Samples, 2024.
- N. Geroliminis, C. F. Daganzo, Existence of urban-scale macroscopic fundamental diagrams: Some experimental findings, *Transportation Research Part B: Methodological* 42 (2008) 759–770. doi:[10.1016/j.trb.2008.02.002](https://doi.org/10.1016/j.trb.2008.02.002).
- V. V. Gayah, C. F. Daganzo, Clockwise hysteresis loops in the Macroscopic Fundamental Diagram: An effect of network instability, *Transportation Research Part B: Methodological* 45 (2011) 643–655. doi:[10.1016/j.trb.2010.11.006](https://doi.org/10.1016/j.trb.2010.11.006).
- N. Geroliminis, J. Sun, Properties of a well-defined macroscopic fundamental diagram for urban traffic, *Transportation Research Part B: Methodological* 45 (2011) 605–617. URL: <http://dx.doi.org/10.1016/j.trb.2010.11.004>. doi:[10.1016/j.trb.2010.11.004](https://doi.org/10.1016/j.trb.2010.11.004).
- H. Mahmassani, T. Hou, M. Saberi, Connecting networkwide travel time reliability and the network fundamental diagram of traffic flow, *Transportation Research Record* (2013) 80–91. doi:[10.3141/2391-08](https://doi.org/10.3141/2391-08).
- T. Tsubota, A. Bhaskar, E. Chung, Macroscopic Fundamental Diagram for Brisbane, Australia, *Transportation Research Record: Journal of the Transportation Research Board* 2421 (2014) 12–21. doi:[10.3141/2421-02](https://doi.org/10.3141/2421-02).
- L. Ambühl, M. Menendez, Data fusion algorithm for macroscopic fundamental diagram estimation, *Transportation Research Part C: Emerging Technologies* 71 (2016) 184–197. doi:[10.1016/j.trc.2016.07.013](https://doi.org/10.1016/j.trc.2016.07.013).

- J. Yang Beibei, H. J. van Zuylen, L. Shoufeng, Determining the Macroscopic Fundamental Diagram on the Basis of Mixed and Incomplete Traffic Data, in: TRB 2016 Annual Meeting, 2016, pp. 1–13.
- J. Du, H. Rakha, V. V. Gayah, Deriving macroscopic fundamental diagrams from probe data: Issues and proposed solutions, *Transportation Research Part C: Emerging Technologies* 66 (2016) 136–149. doi:[10.1016/j.trc.2015.08.015](https://doi.org/10.1016/j.trc.2015.08.015).
- M. Saeedmanesh, N. Geroliminis, Clustering of heterogeneous networks with directional flows based on "Snake" similarities, *Transportation Research Part B: Methodological* 91 (2016) 250–269. doi:[10.1016/j.trb.2016.05.008](https://doi.org/10.1016/j.trb.2016.05.008).
- L. . Ambühl, A. . Loder, M. . Menendez, K. W. Axhausen, Empirical Macroscopic Fundamental Diagrams New insights from loop detector and floating car data (2017). URL: <https://doi.org/10.3929/ethz-b-000167171>. doi:[10.3929/ethz-b-000167171](https://doi.org/10.3929/ethz-b-000167171).
- I. Dakic, M. Menendez, On the use of Lagrangian observations from public transport and probe vehicles to estimate car space-mean speeds in bi-modal urban networks, *Transportation Research Part C: Emerging Technologies* 91 (2018) 317–334. doi:[10.1016/j.trc.2018.04.004](https://doi.org/10.1016/j.trc.2018.04.004).
- G. Mariotte, L. Leclercq, S. F. Batista, J. Krug, M. Paipuri, Calibration and validation of multi-reservoir MFD models: A case study in Lyon, *Transportation Research Part B: Methodological* 136 (2020a) 62–86. doi:[10.1016/j.trb.2020.03.006](https://doi.org/10.1016/j.trb.2020.03.006).
- G. Mariotte, M. Paipuri, L. Leclercq, Dynamics of Flow Merging and Diverging in MFD-Based Systems: Validation vs. Microsimulation, *Frontiers in Future Transportation* 1 (2020b). doi:[10.3389/ffutr.2020.604088](https://doi.org/10.3389/ffutr.2020.604088).
- J. Shim, J. Yeo, S. Lee, S. H. Hamdar, K. Jang, Empirical evaluation of influential factors on bifurcation in macroscopic fundamental diagrams, *Transportation Research Part C: Emerging Technologies* 102 (2019) 509–520. doi:[10.1016/j.trc.2019.03.005](https://doi.org/10.1016/j.trc.2019.03.005).
- H. Fu, Y. Wang, X. Tang, N. Zheng, N. Geroliminis, Empirical analysis of large-scale multimodal traffic with multi-sensor data, *Transportation Research Part C: Emerging Technologies* 118 (2020). doi:[10.1016/j.trc.2020.102725](https://doi.org/10.1016/j.trc.2020.102725).
- S. Jiang, M. Keyvan-Ekbatani, D. Ngoduy, Partitioning of urban networks with polycentric congestion pattern for traffic management policies: Identifying protected networks, *Computer-Aided Civil and Infrastructure Engineering* 38 (2023) 508–527. doi:[10.1111/mice.12895](https://doi.org/10.1111/mice.12895).
- M. Saeedmanesh, N. Geroliminis, Dynamic clustering and propagation of congestion in heterogeneously congested urban traffic networks, *Transportation Research Part B: Methodological* 105 (2017) 193–211. doi:[10.1016/j.trb.2017.08.021](https://doi.org/10.1016/j.trb.2017.08.021).

- Z. Gu, M. Saberi, A bi-partitioning approach to congestion pattern recognition in a congested monocentric city, *Transportation Research Part C: Emerging Technologies* 109 (2019) 305–320. doi:[10.1016/j.trc.2019.10.016](https://doi.org/10.1016/j.trc.2019.10.016).
- M. Johari, S. Jiang, M. Keyvan-Ekbatani, D. Ngoduy, Mode differentiation in partitioning of mixed bi-modal urban networks, *Transportmetrica B* 11 (2023) 463–485. doi:[10.1080/21680566.2022.2089271](https://doi.org/10.1080/21680566.2022.2089271).
- N. Maiti, B. R. Chilukuri, Empirical Investigation of Fundamental Diagrams in Mixed Traffic, *IEEE Access* 11 (2023) 13293–13308. doi:[10.1109/ACCESS.2023.3242971](https://doi.org/10.1109/ACCESS.2023.3242971).
- L. C. Edie, Discussion of traffic stream measurements and definitions, *The 2nd International Symposium on Theory of Traffic flow*, London. 105 (1963) 139–154.
- N. Zheng, N. Geroliminis, On the distribution of urban road space for multi-modal congested networks, *Transportation Research Part B: Methodological* 57 (2013) 326–341. doi:[10.1016/j.trb.2013.06.003](https://doi.org/10.1016/j.trb.2013.06.003).
- E. Saffari, M. Yildirimoglu, M. Hickman, A methodology for identifying critical links and estimating macroscopic fundamental diagram in large-scale urban networks, *Transportation Research Part C: Emerging Technologies* 119 (2020). doi:[10.1016/j.trc.2020.102743](https://doi.org/10.1016/j.trc.2020.102743).
- T. Seo, A. M. Bayen, T. Kusakabe, Y. Asakura, Traffic state estimation on highway: A comprehensive survey, *Annual Reviews in Control* 43 (2017) 128–151. doi:[10.1016/j.arcontrol.2017.03.005](https://doi.org/10.1016/j.arcontrol.2017.03.005).
- A. Takayasu, L. Leclercq, N. Geroliminis, Experimental assessment of traffic density estimation at link and network level with sparse data, *Transportmetrica B* 10 (2022) 368–395. doi:[10.1080/21680566.2021.2002738](https://doi.org/10.1080/21680566.2021.2002738).
- X. Wu, H. X. Liu, N. Geroliminis, An empirical analysis on the arterial fundamental diagram, *Transportation Research Part B: Methodological* 45 (2011) 255–266. URL: <http://dx.doi.org/10.1016/j.trb.2010.06.003>. doi:[10.1016/j.trb.2010.06.003](https://doi.org/10.1016/j.trb.2010.06.003).
- A. Nantes, D. Ngoduy, A. Bhaskar, M. Miska, E. Chung, Real-time traffic state estimation in urban corridors from heterogeneous data, *Transportation Research Part C: Emerging Technologies* 66 (2016) 99–118. doi:[10.1016/j.trc.2015.07.005](https://doi.org/10.1016/j.trc.2015.07.005).
- N. Maiti, B. R. Chilukuri, Estimation of local traffic conditions using Wi-Fi sensor technology, *Journal of Intelligent Transportation Systems* 28 (2024) 618–635. doi:[10.1080/15472450.2023.2177103](https://doi.org/10.1080/15472450.2023.2177103).
- N. Maiti, J. A. Laval, B. R. Chilukuri, Universality of area occupancy-based fundamental diagrams in mixed traffic, *Physica A: Statistical Mechanics and its Applications* 640 (2024). doi:[10.1016/j.physa.2024.129692](https://doi.org/10.1016/j.physa.2024.129692).

- N. Maiti, B. R. Chilukuri, Does anisotropy hold in mixed traffic conditions?, *Physica A: Statistical Mechanics and its Applications* 632 (2023) 129336. doi:[10.1016/j.physa.2023.129336](https://doi.org/10.1016/j.physa.2023.129336).
- Qing-Jie Kong, Zhipeng Li, Yikai Chen, Yuncai Liu, An Approach to Urban Traffic State Estimation by Fusing Multisource Information, *IEEE Transactions on Intelligent Transportation Systems* 10 (2009) 499–511. doi:[10.1109/TITS.2009.2026308](https://doi.org/10.1109/TITS.2009.2026308).
- K. Anuar, F. Habtemichael, M. Cetin, Estimating Traffic Flow Rate on Freeways from Probe Vehicle Data and Fundamental Diagram, in: *2015 IEEE 18th International Conference on Intelligent Transportation Systems*, IEEE, 2015, pp. 2921–2926. doi:[10.1109/ITSC.2015.468](https://doi.org/10.1109/ITSC.2015.468).
- S. Lu, V. L. Knoop, M. Keyvan-Ekbatani, Using taxi GPS data for macroscopic traffic monitoring in large scale urban networks: Calibration and MFD derivation, in: *Transportation Research Procedia*, volume 34, Elsevier B.V., 2018, pp. 243–250. doi:[10.1016/j.trpro.2018.11.038](https://doi.org/10.1016/j.trpro.2018.11.038).
- C. Chen, J. Kwon, J. Rice, A. Skabardonis, P. Varaiya, Detecting Errors and Imputing Missing Data for Single-Loop Surveillance Systems, *Transportation Research Record: Journal of the Transportation Research Board* 1855 (2003) 160–167. doi:[10.3141/1855-20](https://doi.org/10.3141/1855-20).
- D. W. Xu, H. H. Dong, H. J. Li, L. M. Jia, Y. J. Feng, The estimation of road traffic states based on compressive sensing, *Transportmetrica B: Transport Dynamics* 3 (2015) 131–152. doi:[10.1080/21680566.2014.963736](https://doi.org/10.1080/21680566.2014.963736).
- K. J. Ofor, L. Vaci, L. S. Mihaylova, Traffic Estimation for Large Urban Road Network with High Missing Data Ratio, *Sensors* 19 (2019) 2813. doi:[10.3390/s19122813](https://doi.org/10.3390/s19122813).
- E. Rossi, H. Kenlay, M. I. Gorinova, B. P. Chamberlain, X. Dong, M. Bronstein, On the Unreasonable Effectiveness of Feature propagation in Learning on Graphs with Missing Node Features (2021). URL: <http://arxiv.org/abs/2111.12128>.
- H. Taguchi, X. Liu, T. Murata, Graph convolutional networks for graphs containing missing features, *Future Generation Computer Systems* 117 (2021) 155–168. doi:[10.1016/j.future.2020.11.016](https://doi.org/10.1016/j.future.2020.11.016).
- J. A. Castro-Correa, J. H. Giraldo, A. Mondal, M. Badiey, T. Bouwmans, F. D. Malliaros, Time-varying Signals Recovery via Graph Neural Networks (2023). URL: <http://arxiv.org/abs/2302.11313><http://dx.doi.org/10.1109/ICASSP49357.2023.10096168>. doi:[10.1109/ICASSP49357.2023.10096168](https://doi.org/10.1109/ICASSP49357.2023.10096168).
- Y. Bao, J. Liu, Q. Shen, Y. Cao, W. Ding, Q. Shi, PKET-GCN: Prior knowledge enhanced time-varying graph convolution network for traffic flow prediction, *Information Sciences* 634 (2023) 359–381. doi:[10.1016/j.ins.2023.03.093](https://doi.org/10.1016/j.ins.2023.03.093).

- J. Zhang, C. Song, S. Cao, C. Zhang, FDST-GCN: A Fundamental Diagram based Spatiotemporal Graph Convolutional Network for expressway traffic forecasting, *Physica A: Statistical Mechanics and its Applications* 630 (2023). doi:[10.1016/j.physa.2023.129173](https://doi.org/10.1016/j.physa.2023.129173).
- Y. Zhang, B. Chen, S. Wang, J. Cao, GCGAN: Generative Adversarial Nets with Graph CNN for Network-Scale Traffic Prediction, in: 19. International Joint Conference on Neural Networks. Budapest, Hungary., IEEE, 2019. URL: <http://www.ieee.org/publications>.
- H. Zheng, X. Li, Y. Li, Z. Yan, T. Li, GCN-GAN: Integrating Graph Convolutional Network and Generative Adversarial Network for Traffic Flow Prediction, *IEEE Access* 10 (2022) 94051–94062. doi:[10.1109/ACCESS.2022.3204036](https://doi.org/10.1109/ACCESS.2022.3204036).
- J. Zhang, S. Mao, L. Yang, W. Ma, S. Li, Z. Gao, Physics-informed deep learning for traffic state estimation based on the traffic flow model and computational graph method, *Information Fusion* 101 (2024). doi:[10.1016/j.inffus.2023.101971](https://doi.org/10.1016/j.inffus.2023.101971).
- M. Usama, R. Ma, J. Hart, M. Wojcik, Physics-Informed Neural Networks (PINNs)-Based Traffic State Estimation: An Application to Traffic Network, *Algorithms* 15 (2022). doi:[10.3390/a15120447](https://doi.org/10.3390/a15120447).
- J. K. Eom, M. S. Park, T.-Y. Heo, L. F. Huntsinger, Improving the Prediction of Annual Average Daily Traffic for Nonfreeway Facilities by Applying a Spatial Statistical Method, *Transportation Research Record: Journal of the Transportation Research Board* 1968 (2006) 20–29. doi:[10.1177/0361198106196800103](https://doi.org/10.1177/0361198106196800103).
- X. Wang, K. M. Kockelman, Forecasting Network Data, *Transportation Research Record: Journal of the Transportation Research Board* 2105 (2009) 100–108. doi:[10.3141/2105-13](https://doi.org/10.3141/2105-13).
- H. Zou, Y. Yue, Q. Li, A. G. Yeh, An improved distance metric for the interpolation of link-based traffic data using kriging: a case study of a large-scale urban road network, *International Journal of Geographical Information Science* 26 (2012) 667–689. doi:[10.1080/13658816.2011.609488](https://doi.org/10.1080/13658816.2011.609488).
- B. Selby, K. M. Kockelman, Spatial prediction of traffic levels in unmeasured locations: applications of universal kriging and geographically weighted regression, *Journal of Transport Geography* 29 (2013) 24–32. doi:[10.1016/j.jtrangeo.2012.12.009](https://doi.org/10.1016/j.jtrangeo.2012.12.009).
- J. Yang, L. D. Han, P. B. Freeze, S.-M. Chin, H.-L. Hwang, Short-Term Freeway Speed Profiling Based on Longitudinal Spatiotemporal Dynamics, *Transportation Research Record: Journal of the Transportation Research Board* 2467 (2014) 62–72. doi:[10.3141/2467-07](https://doi.org/10.3141/2467-07).



- D. Marcotte, Cokriging with matlab, *Computers & Geosciences* 17 (1991) 1265–1280. doi:[10.1016/0098-3004\(91\)90028-C](https://doi.org/10.1016/0098-3004(91)90028-C).
- B. Shamo, E. Asa, J. Membah, Linear Spatial Interpolation and Analysis of Annual Average Daily Traffic Data, *Journal of Computing in Civil Engineering* 29 (2015). doi:[10.1061/\(asce\)cp.1943-5487.0000281](https://doi.org/10.1061/(asce)cp.1943-5487.0000281).
- B. Bae, H. Kim, H. Lim, Y. Liu, L. D. Han, P. B. Freeze, Missing data imputation for traffic flow speed using spatio-temporal cokriging, *Transportation Research Part C: Emerging Technologies* 88 (2018) 124–139. doi:[10.1016/j.trc.2018.01.015](https://doi.org/10.1016/j.trc.2018.01.015).
- J. Laval, Traffic Flow as a Simple Fluid: Towards a Scaling Theory of Urban Congestion, *Transportation Research Record: Journal of the Transportation Research Board* (2023). doi:[10.1177/03611981231179703](https://doi.org/10.1177/03611981231179703).
- D. Krige, A statistical approach to some basic mine valuation problems on the Witwatersrand, *Journal of the Southern African Institute of Mining and Metallurgy* 52 (1951).
- G. Matheron, Principles of geostatistics, *Economic Geology* 58 (1963) 1246–1266. doi:[10.2113/gsecongeo.58.8.1246](https://doi.org/10.2113/gsecongeo.58.8.1246).
- N. Cressie, *Statistics for spatial data*, John Wiley, New York Publication country United States, 1993.
- M. A. R. W. Oliver, *A tutorial guide to geostatistics: Computing and modelling variograms and kriging*, volume 113, Catena, 2014.